American Mineralogist, Volume 88, pages 277–287, 2003

Hydrogen-bonded water in laumontite I: X-ray powder diffraction study of water site occupancy and structural changes in laumontite during room-temperature isothermal hydration/dehydration

THRÁINN FRIDRIKSSON,[1,*] DAVID L. BISH,[2] AND DENNIS K. BIRD[1]

[1]Department of Geological and Environmental Sciences, Stanford University, Stanford, California 94305-2115, U.S.A.
[2]Hydrology, Geochemistry, and Geology, MS D469, Los Alamos National Laboratory, Los Alamos, New Mexico 87545, U.S.A.

ABSTRACT

The response of the laumontite crystal structure to hydration/dehydration was evaluated using Rietveld refinements with XRD data collected under controlled P_{H_2O} conditions at ~28.5 °C. Refined water contents per unit cell (unit-cell formula: $Ca_4Al_8Si_{16}O_{48}{\cdot}nH_2O$) ranged between 12.5 H_2O at 0.11 mbar P_{H_2O} and 17.3 H_2O at 37.6 mbar. The occupancy of the two water sites hosting hydrogen-bonded water molecules, W5 and W1, ranged from 13% to 100% and from 2% to 86%, respectively. During hydration of W5, between 0.11 and 5 mbar, the unit cell expanded continuously and reversibly from 1327 to 1348 Å^3. The unit-cell volume remained nearly constant between 5 and 28 mbar. The hydration/dehydration of W1 exhibited hysteresis; hydration occurred at ~29 mbar and dehydration at ~24 mbar. During hydration of W1 at ~29 mbar the unit cell expanded from 1351 to 1384 Å^3. Further hydration of W1 above 29 mbar resulted in gradual and reversible unit-cell expansion to 1386 Å^3 at 37.6 mbar. Hydration/dehydration of W5 is a continuous reaction typical for zeolites. In contrast, the hydration/dehydration of W1 at room temperature is discontinuous, as manifested by the presence of two laumontite phases during hydration and dehydration. Unit-cell parameters of the two coexisting laumontite phases observed under these conditions are consistent with a vacant W1 site and ~80%-occupied W1 site, respectively. Gradual unit-cell expansion above 29 mbar due to increased P_{H_2O} and increased occupancy of W1 indicate that hydration of the remaining 20% of the W1 site proceeds continuously.

INTRODUCTION

Laumontite, $Ca_4Al_8Si_{16}O_{48}{\cdot}nH_2O$, is a common rock-forming zeolite occurring world wide as a secondary mineral in low-grade metavolcanic (e.g., Sukheswala et al. 1974; Murata et al. 1987; Schmidt 1990; Neuhoff et al. 1997, 1999, 2000; Fridriksson et al. 2001) and volcanically derived sedimentary rocks (e.g., Coombs et al. 1959; Iijima 1978, 1988). Laumontite is an index mineral for higher-grade zeolite facies metamorphism as defined by Coombs et al. (1959). Similarly, the highest-grade zeolite zone in regionally metamorphosed basalts is defined by the presence of laumontite as the most common zeolite species (Sukheswala et al. 1974; Murata et al. 1987; Schmidt 1990; Neuhoff et al. 2000).

Predictive modeling of mineral parageneses in geologic systems and evaluation of the stability and performance of zeolites in industrial applications requires careful consideration of zeolite water stoichiometry and the thermodynamic properties of zeolitic water. A recent study by Neuhoff and Bird (2001) on laumontite dehydration illustrated the importance of this point. Using available experimental and field observations, they demonstrated that natural and experimentally observed zeolite phase relations are not compatible with the water stoichiometry of fully hydrated laumontite ($Ca_4Al_8Si_{16}O_{48}{\cdot}18H_2O$). Instead, they require the water stoichiometry of partially dehydrated laumontite formerly referred to as "leonhardite" ($Ca_4Al_8Si_{16}O_{48}{\cdot}14H_2O$; leonhardite was discredited by the IMA Subcommittee on Zeolites, Coombs et al. 1997, and we refer to it in this communication within quotes).

The X-ray diffraction (XRD) study presented in this contribution is a part of an integrated XRD, thermogravimetric (TGA), and calorimetric investigation of the properties of hydrogen-bonded water molecules in laumontite. Our objective is to provide thermodynamic data necessary to predict the water content of individual sites in laumontite at temperatures and pressures relevant to zeolite parageneses. In this contribution, we present crystal structural data required for quantitative interpretation of TGA and calorimetric experiments that will be presented in a separate communication. Specific objectives of the present study include determination of water site occupancies as a function of water-vapor pressure at room temperature and investigation of mechanisms of hydration and dehydration reactions for individual water sites. When combined with results of TGA and calorimetric experiments, the structural data presented here provide information on the effects of near atomic environment on the thermodynamic properties of zeolitic water.

CRYSTAL CHEMICAL BACKGROUND

Fully hydrated laumontite contains 18 water molecules per unit cell (Yamazaki et al. 1991; Armbruster and Kohler 1992;

* E-mail: thrainn@pangea.stanford.edu

Artioli and Ståhl 1993; Ståhl and Artioli 1993; Ståhl et al. 1996). When exposed to air (~50% relative humidity, *RH*) at room temperature, laumontite loses four water molecules (Yamazaki et al. 1991), resulting in "leonhardite" stoichiometry with 14 water molecules per unit cell (Coombs 1952). Further drying at room temperature (<5% *RH*) results in the loss of two more water molecules per unit cell ($Ca_4Al_8Si_{16}O_{48}\cdot 12H_2O$; Yamazaki et al. 1991). Recent crystal-structure refinements have shown that 12 of the 18 water molecules in the laumontite unit cell are associated with the extraframework Ca^{2+} ions, whereas the remaining six are hydrogen bonded to framework O atoms and the water molecules hydrating Ca^{2+} (Artioli et al. 1989; Armbruster and Kohler 1992; Artioli and Ståhl 1993; Ståhl and Artioli 1993; Ståhl et al. 1996). Crystal-structure refinements using single-crystal neutron diffraction data measured at 15 K (Artioli et al. 1989) and single-crystal X-ray diffraction data measured at 100 K (Armbruster and Kohler 1992) have identified 11 and 7 distinct water sites in laumontite, respectively. However, some of these sites merge at higher temperatures, resulting in only four distinct water sites at and above room temperature (Artioli and Ståhl 1993; Ståhl and Artioli 1993; Ståhl et al. 1996) referred to as W1, W2, W5, and W8 (after Artioli et al. 1989). Two of these sites, W2 and W8 (containing four and eight water molecules per unit cell, respectively), solvate the Ca^{2+} ion. The remaining two, W1 and W5 (containing four and two water molecules per unit cell, respectively, in fully hydrated laumontite) are hydrogen bonded to framework O atoms and other water molecules. The four water sites are illustrated in Figure 1, which depicts the crystal structures of a fully hydrated laumontite and two partially dehydrated laumontites.

Ståhl et al. (1996) demonstrated by Rietveld refinements, using powder XRD data collected during stepwise heating of laumontite, that the water sites dehydrate sequentially. Most of the water at W1 was lost at 76 °C, while the remaining water sites remained fully occupied. Upon further heating, 80% of the water at W5 was lost at ~100 °C, and at 207 °C 80% of the water at W2 was released. These observations are consistent with the results of room-temperature gravimetric experiments under controlled-*RH* conditions reported by Yamazaki et al. (1991) who found that zeolitic water is lost from laumontite in two abrupt steps. The sequence and stoichiometry of the hydration/dehydration steps reported by Yamazaki et al. (1991) suggest, by analogy to the results of Ståhl et al. (1996), that one step involves only the two water molecules on W5 and the other involves the four water molecules on W1.

Stepwise hydration/dehydration of laumontite, involving only one water site at each step, is a manifestation of the distinctly different energetic properties of these sites. This contrasts with the situation found in many other zeolites, in which a variety of energetically similar water sites exist. Therefore, laumontite provides an excellent opportunity to investigate the properties of individual water sites in a zeolite structure. Experimental observations allowing evaluation of the thermodynamic properties of the W1 site already exist. These include measurements of the enthalpy of hydration of fully hydrated laumontite and "leonhardite" by transposed temperature-dropsolution calorimetry (Kiseleva et al. 1996) and calorimetric measurements of the low-temperature heat capacity of

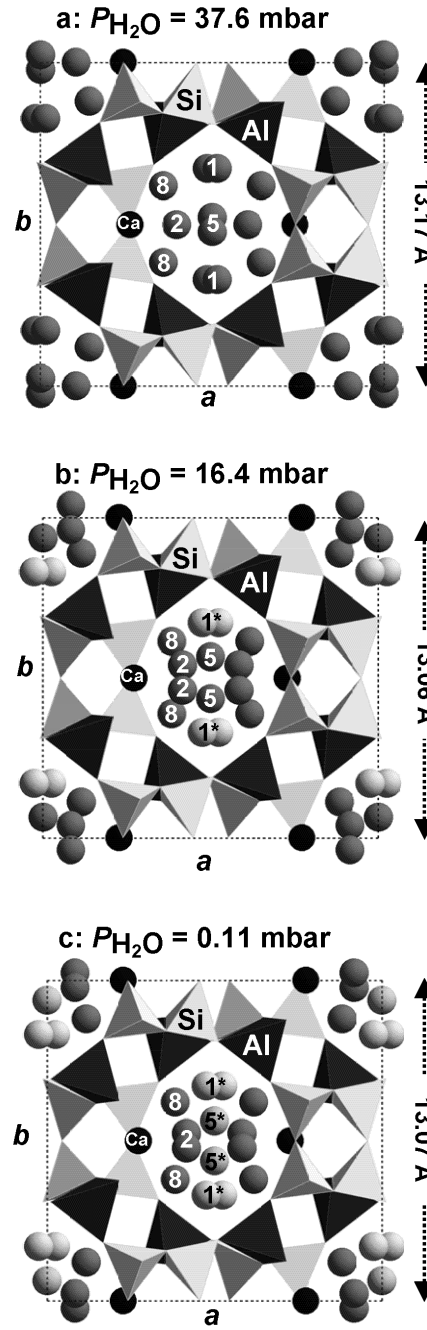

FIGURE 1. Crystal structures of fully hydrated and partially dehydrated laumontite. The diagrams show the view along the *c* axis of the crystal structure for (**a**) fully hydrated laumontite at 37.6 mbar P_{H_2O}, (**b**) laumontite with W1 vacant and W2, W5, and W8 occupied at 16.4 mbar, and (**c**) with W1 and W5 nearly vacant and W2 and W8 occupied at 0.11 mbar. The crystal structure models were constructed using the data in Tables 2–4. Water sites are shown as gray-shaded spheres; occupied sites are shown as dark gray and near-vacant sites are shown as lighter shades of gray depending on their fractional occupancy. The water sites W1, W2, W5, and W8 are labeled 1, 2, 5, and 8, respectively, and vacant or near-vacant sites are denoted by a star (*). Ca^{2+} ions are shown as black spheres. The Si-bearing tetrahedra are light colored and Al-bearing tetrahedra are dark.

laumontite and "leonhardite" (Paukov and Fursenko 1998a, 1998b). It can be inferred from the above structural observations and the reported water content of the experimental materials of Kiseleva et al. (1996) and Paukov and Fursenko (1998a, 1998b) that the laumontite and "leonhardite" stoichiometries represent samples with fully occupied W1 and empty W1 sites, respectively. According to the results of Kiseleva et al. (1996), the molar enthalpy of hydration of W1 referenced to liquid water at 25 °C is –6.4 ± 9.2 kJ/mol, whereas the average molar enthalpy of hydration for the remaining water (W2, W5, and W8) is ~ –40 kJ/mol.

Experimental setup

The laumontite sample used in this study is from Drain County, Oregon. The composition of the sample, $Ca_{3.88}Na_{0.15}K_{0.03}Al_{8.00}Si_{16.00}O_{48}\cdot nH_2O$, is an average of 28 electron microprobe analyses of several different grains. Analyses were performed using a Cameca SX50 electron microprobe with accelerating voltage of 15.0 kV, a beam current of 15.0 nA, and a beam diameter of 10 µm. Zeolitic water was determined by difference between 100% and the sum of the analyzed oxide weight percents and was accounted for in the PAP matrix corrections (Pouchou and Pichoir 1984). The sample is chemically homogenous; the standard deviations of Ca and Na were 0.12 moles per unit-cell formula. The maximum water content of the sample at 24 °C and 100% *RH* was 18.04 moles of H_2O per unit-cell formula, as determined by thermogravimetric analysis. Laumontite crystals (1 to 4 mm) for diffraction and thermal studies were handpicked from the natural sample and ground in a Spex shatterbox. The ~2 to 10 µm size fraction was separated by repeated centrifuging in water.

XRD patterns were measured with an automated Siemens D500 diffractometer with incident- and diffracted-beam Soller slits, a Kevex solid-state Si(Li) detector, and Cu$K\alpha$ radiation. The diffractometer was calibrated using NIST SRM 640b Si. The diffractometer was equipped with a specially designed environmental chamber (Chipera et al. 1997) that allows precise control of relative humidity (*RH*) and consequently the P_{H_2O} of the atmosphere surrounding the sample. Desired *RH* was obtained by mixing dry N_2 gas with water-saturated N_2 gas using automated mass-flow controllers. The *RH* was measured inside the sample chamber with a calibrated capacitance-film hygrometer probe. An automated feedback loop, using the *RH* readings of the probe in the sample chamber, controlled the respective flow rates of the two gases, maintaining a constant total gas flow of 200 cm^3/s. XRD data were collected at temperatures between 27.0 and 29.3 °C. During individual experiments the measured temperature inside the sample chamber varied by ≤0.1 °C.

X-ray diffraction data for Rietveld refinements of atom positions and water site occupancies were collected at 0.29 ± 0.1%, 1.2 ± 0.2%, 3.1 ± 0.2%, 41.7 ± 0.5%, 68.4 ± 0.2%, 73.4 ± 0.7%, and 94.4 ± 0.7% *RH*, corresponding to 0.11, 0.66, 1.2, 16.4, 25.3, 27.0, and 37.6 mbar P_{H_2O}, respectively, at the experimental temperatures. The sample was equilibrated prior to data collection for at least 150 minutes at 1.2, 16.4, 25.3, 27.0, and 37.6 mbar, for 500 minutes at 0.66 mbar, and for 1500 minutes at 0.11 mbar. Longer equilibration times were used at lower water-vapor pressures because complete drying of the sample chamber is slow. To ensure maximum hydration of the sample at 27.0 mbar it was equilibrated at 35 mbar for 2 hours prior to equilibration at 27.0 mbar. Each data set consisted of two or three diffraction patterns, either measured from 2 to 50° 2θ counting for 4 s per step and from 50 to 150° 2θ counting for 44 s per step or from 2 to 26° 2θ counting for 2 s per step, from 26 to 50° 2θ counting for 10 s per step, and from 50 to 104° 2θ counting for 20 s per step. In all cases the step size was 0.02° 2θ. In addition, several XRD patterns for Rietveld refinements of unit-cell parameters were measured at water-vapor pressures ranging from 0.5 mbar to 35 mbar. These patterns were measured from 8 to 79° 2θ, counting for 1 s at each 0.02° 2θ step after an equilibration time of 2 hours at the given *RH*.

Rietveld refinements

Rietveld refinements were performed using the GSAS software package (Larson and von Dreele 2000), using the W1-vacant structure reported by Ståhl et al. (1996) for a laumontite submerged in water at 367 K as a starting model for refinement of the laumontite structure at 16.4 mbar P_{H_2O}. The resulting structure was used as the starting model for subsequent refinements of the laumontite structure at 0.11, 0.66, 1.2, and 25.3 mbar. The structure reported by Ståhl et al. (1996) for laumontite submerged in water at 310 K (nearly completely hydrated) was used as the starting model for refinement of the laumontite structure at 27.0 and 37.6 mbar. All refinements were carried out in space group $C2/m$ in accord with Artioli et al. (1989) and Armbruster and Kohler (1992). The distribution of Al and Si atoms at the tetrahedral sites was assumed to be fully ordered, in accord with Artioli et al. (1989) and Armbruster and Kohler (1992). Near complete ordering of the experimental material was confirmed by ^{29}Si MAS NMR experiments (P.S. Neuhoff, personal communication).

Two or three data sets (histograms; 2–50 and 50–150° 2θ or 2–26, 26–50, and 50–104° 2θ) were used for refinement, constraining the scale factors for each histogram to the ratios of their respective count times. Observations below 18° 2θ were excluded from the refinements. We used the cosine Fourier-series background function and the pseudo-Voigt profile function. The contributions of anisotropic microstrain and crystallite size to peak broadening were refined. Peak broadening due to crystallite size was negligible, but the effects of anisotropic microstrain were moderate but significant (see below). Preferred orientation was modeled using a spherical harmonics correction. The refined texture index was between 1.12 and 1.21, indicating only minor preferential orientation of the powder sample.

Atomic coordinates and isotropic displacement factors (U_{iso}) were refined for all atoms of the tetrahedral framework and the extraframework Ca^{2+} ion. In some cases, refined isotropic displacement factors were negative for one or more of the framework O atoms and in one instance a Si atom had a negative refined U_{iso} value. In these cases, the displacement factors were constrained to be equal for all atoms of the same type. Soft constraints were applied to the Si-O and Al-O bond distances using 1.603 ± 0.02 Å and 1.76 ± 0.03 Å for the Si-O and Al-O bond distances, respectively (Alberti and Gottardi 1988). The soft constraints accounted for less than 2% of the total minimi-

zation function in all refinements. The occupancies of the water sites, W1, W2, W5, and W8, were refined, and atomic coordinates for the water O atoms were refined for water sites with greater than 20% occupancy. In all cases, the refined occupancy of W2, and occasionally of W8 and W5, exceeded the maximum water content for those sites by 5 to 10%. In these cases, the water content of the respective sites was fixed to be equal to the maximum occupancy. Simultaneous refinement of water site occupancies and isotropic displacement factors was successful in some cases. However, when correlation prevented simultaneous refinement of realistic values for these parameters they were refined alternatively, i.e., occupancies were refined while thermal displacement factors were held constant and vice versa until convergence was achieved.

Fourier difference maps (calculated after constraining the occupancy of individual water sites to zero) suggested that the occupied water sites are generally spherical in shape and were thus properly modeled by isotropic displacement factors. The exception to this was W8, which exhibited elongation in the 16.4 and 25.3 mbar P_{H_2O} structure models. Figure 2 depicts a Fourier map of a spherical W8 site in the 37.6 mbar structure, an elongated W8 site for the 16.4 mbar structure, and the W5 site in the 16.4 mbar structure. The use of anisotropic displacement factors for W8 yielded moderately improved refinement statistics for the structures at 16.4 and 25.3 mbar (R_{wp} decreased by 6.8% and 4.4%, respectively; see footnote to Table 1 for definition of R_{wp}). The use of anisotropic displacement factors for W8 improved the refinement statistics for the 27.0 and the 37.6 mbar structures only slightly but had a negligible effect on the refinement statistics for the 0.11, 0.66, and 1.2 mbar refinements. Consequently, the W8 site was modeled with anisotropic displacement factors in the structure models at 16.4 and 25.3 mbar but with isotropic displacement factors in the remaining five refinements. Table 1 lists the refined unit-cell parameters, refined water contents, and selected statistical parameters describing the overall fit of the refinements. Refined atomic coordinates, site occupancies, and isotropic displacement factors (and anisotropic displacement factors for W8) for laumontite at 0.11, 16.4, and 37.6 mbar are listed in Tables 2, 3, and 4, respectively.

The structures of laumontite at 0.11, 16.4, and 37.6 mbar P_{H_2O} were used as starting models for Rietveld refinements of unit-cell parameters (Figs. 3 and 4). The 0.11 mbar structure (Table 2) was used for refinements of unit-cell parameters below 2.5 mbar. The 16.4 mbar structure (Table 3) was used for refinements of unit-cell parameters between 2.5 and 29 mbar on hydration and 2.5 and 24 mbar on dehydration. The 37.6 mbar structure (Table 4) was used for unit-cell parameter refinements above 29 mbar during hydration and 25 mbar during dehydration. At ~28 mbar on hydration and ~25 mbar on dehydration the XRD pattern showed split reflections, i.e., reflections from two laumontite phases with different unit-cell parameters (Fig. 5). In those cases, unit-cell parameters were refined for two laumontite phases, one with the 16.4 mbar structure as a starting model and the other with the 37.6 mbar structure as a starting model. During refinements of unit-cell parameters, background, phase fraction, preferential orientation, and sample displacement were varied along with unit-cell parameters.

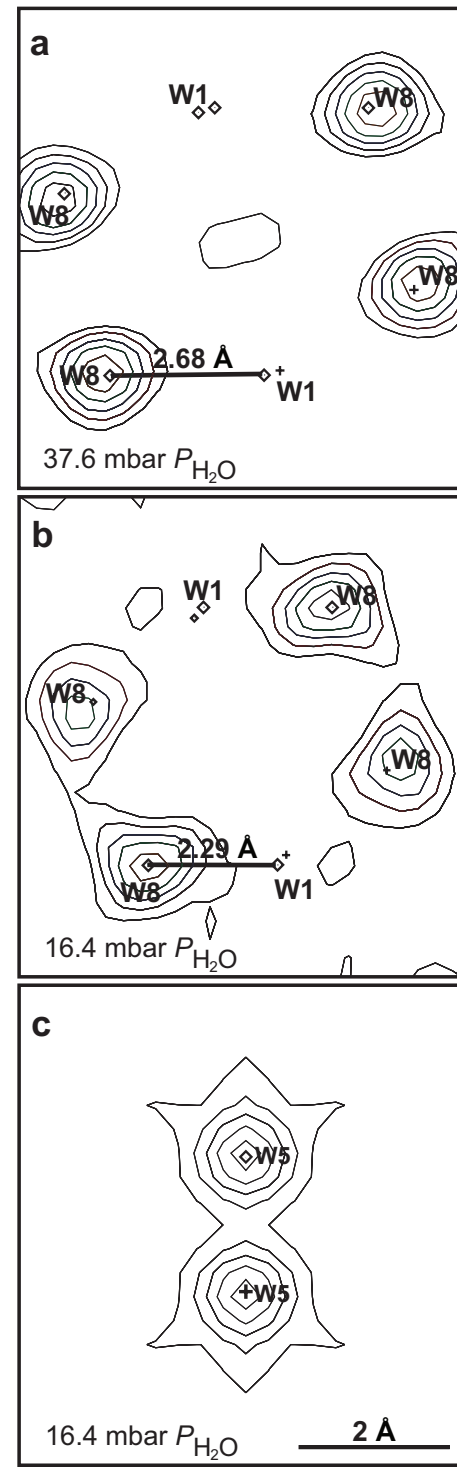

FIGURE 2. Fourier difference maps, calculated after setting the occupancy of individual water sites equal to zero, showing (**a**) the W8 site in the 37.6 mbar structure, (**b**) the W8 site in the 16.4 mbar structure, and (**c**) the W5 site in the 16.4 mbar structure. Note the spherical shape of W8 in the 37.5 mbar structure (**a**) and of W5 (**c**) and the elongation of W8 toward the vacant W1 in the 16.4 mbar structure (**b**). Note also that the distance between the center of W8 site and the empty W1 site in (**b**) is less than the minimum distance between two occupied water sites.

TABLE 1. Refinement summary

P_{H_2O}	0.11 mbar	0.66 mbar	1.2 mbar	16.4 mbar	25.3 mbar	27.0 mbar	37.6 mbar
Temperature (°C)	27.9	28.7	27.7	29.3	27.6	27.5	28.9
a (Å)	14.70542(1)	14.71565(2)	14.7356(1)	14.74716(1)	14.74820(1)	14.8494(2)	14.8786(2)
b (Å)	13.07118(8)	13.06712(1)	13.06520(9)	13.06601(1)	13.06981(8)	13.1792(1)	13.1708(2)
c (Å)	7.45156(8)	7.4649(1)	7.49962(9)	7.55735(8)	7.55869(7)	7.53672(9)	7.5373(1)
β (°)	112.121(1)	112.109(1)	112.069(1)	112.0399(6)	112.014(1)	110.505(1)	110.196(1)
Volume (Å^3)	1326.89(2)	1329.89(3)	1338.07(2)	1349.79(2)	1350.76(2)	1381.52(3)	1386.22(4)
nH_2O (per unit cell)	12.50(4)	12.70(4)	13.89(5)	14.09(7)	14.04(6)	17.16(5)	17.29(5)
R_{wp}*	0.061	0.080	0.069	0.060	0.056	0.069	0.084
R_p†	0.046	0.061	0.052	0.047	0.043	0.052	0.064
Reduced χ^2‡	6.80	6.28	8.834	3.64	5.80	8.72	7.20
R (Bragg) § histogram 1	0.056	0.066	0.069	0.025	0.054	0.067	0.0423
R (Bragg) § histogram 2	0.032	0.036	0.033	0.028	0.038	0.038	0.0444
R (Bragg) § histogram 3		0.032		0.034			0.0487
Number of variables	87	88	88	93	90	82	95
Number of observations	6610	4297	6610	4309	6610	6611	4292
Number of reflections	3052	1502	3324	1729	3117	3544	1674

Notes: I_o and I_c, refer to observed and calculated intensities at a given 2θ step. The subscript *k* refers to Bragg reflections.

* $R_{wp} = \sqrt{\frac{\sum \left| I_o - I_c \right|^2}{\sum w I_o^2}}$. † $R_p = \frac{\sum |I_o - I_c|}{\sum I_o}$. ‡ $\text{Reduced } \chi^2 = \frac{\sum |I_o - I_c|}{N_{obs} - N_{var}}$. § $R_{Bragg} = \frac{\sum |I_{ko} - I_{kc}|}{\sum I_{ko}}$.

TABLE 2. Laumontite structure at 0.11 mbar P_{H_2O}

Atom	*x*	*y*	*z*	Occupancy	U_{iso}
Si1	0.23740(11)	0.38250(11)	0.15688(26)	1.00	0.00108(34)
Si2	0.07813(10)	0.38454(11)	0.31593(27)	1.00	0.00125(33)
Al	0.13040(11)	0.30946(12)	0.72981(28)	1.00	0.0004(4)
O1	0.25780(41)	0.50	0.2346(9)	1.00	0.0038(4)
O2	0.21509(24)	0.37643(29)	0.9277(5)	1.00	0.0038(4)
O3	0.14697(24)	0.38502(30)	0.5461(5)	1.00	0.0038(4)
O4	0.14338(25)	0.34208(25)	0.1982(6)	1.00	0.0038(4)
O5	0.33276(24)	0.31728(25)	0.2794(7)	1.00	0.0038(4)
O6	0.04374(35)	0.50	0.2497(9)	1.00	0.0038(4)
O7	0.01177(22)	0.30891(29)	0.7235(7)	1.00	0.0038(4)
Ca	0.27328(13)	0.50	0.75034(31)	1.00	0.0069(4)
W1	0.025	0.17	0.00	0.030(7)	0.0192(26)
W2	0.41694(52)	0.47696(58)	0.0589(13)	0.50	0.0192(26)
W5	0.50	0.4378	0.50	0.066(13)	0.0317(13)
W8	0.11752(34)	0.12007(36)	0.3205(8)	1.00	0.0317(13)

TABLE 3. Laumontite structure at 16.4 mbar P_{H_2O}

Atom	*x*	*y*	*z*	Occupancy	U_{iso}
Si1	0.23817(13)	0.38214(12)	0.15752(29)	1.00	0.0047(5)
Si2	0.08328(12)	0.38332(12)	0.32681(28)	1.00	0.0038(5)
Al	0.12850(12)	0.31001(14)	0.73388(29)	1.00	0.0046(6)
O1	0.26062(38)	0.50	0.2272(9)	1.00	0.0077(5)
O2	0.20980(25)	0.37876(29)	0.9291(4)	1.00	0.0077(5)
O3	0.14738(26)	0.38453(28)	0.5544(4)	1.00	0.0077(5)
O4	0.14923(23)	0.34054(27)	0.2133(5)	1.00	0.0077(5)
O5	0.33694(22)	0.31729(24)	0.2700(7)	1.00	0.0077(5)
O6	0.05190(34)	0.50	0.2621(8)	1.00	0.0077(5)
O7	0.00863(21)	0.30915(28)	0.7201(6)	1.00	0.0077(5)
Ca	0.27194(13)	0.50	0.75867(32)	1.00	0.0126(6)
W1	0.025	0.17	0.00	0.011(5)	0.0469(35)
W2	0.41577(61)	0.46147(56)	0.0573(15)	0.50	0.0469(35)
W5	0.50	0.43509(84)	0.50	0.50	0.0557(47)
W8	0.11622(34)	0.11218(40)	0.3000(11)	1.00	*

* Anisotropic displacement factors for W8 are: U_{11} = 0.0339(44), U_{22} = 0.091(5), U_{33} = 0.226(11), U_{12} = 0.008(4), U_{13} = 0.047(6), U_{23} = –0.091(6).

RESULTS

Rietveld refinements of laumontite crystal structure as a function of P_{H_2O}

The tetrahedral framework topologies refined in this study (Tables 2 to 4) are in close agreement with earlier structure refinements of laumontite at and below room temperature (Artioli et al. 1989; Armbruster and Kohler 1992; Artioli and Ståhl 1993; Ståhl and Artioli 1993). The T-O-T angles (tetrahedral cation–O atom–tetrahedral cation) observed in this study are all within 2° of the T-O-T angles reported by Armbruster and Kohler (1992) for structures with comparable water contents. The T-O-T angles at ~14 H_2O per unit cell are generally within a few tenths of a percent of those reported by Artioli et al. (1989) for that water content, with the exception of Si2-O3-

TABLE 4. Laumontite structure at 37.6 mbar P_{H_2O}

Atom	*x*	*y*	*z*	Occupancy	U_{iso}
Si1	0.23594(20)	0.38305(21)	0.1507(4)	1.00	0.01077(87)
Si2	0.07851(19)	0.38374(18)	0.3254(4)	1.00	0.00757(79)
Al	0.12877(20)	0.30795(20)	0.7362(5)	1.00	0.01049(97)
O1	0.2586(60)	0.50	0.2202(13)	1.00	0.0107(26)
O2	0.2094(4)	0.3790(4)	0.9242(6)	1.00	0.0106(17)
O3	0.1391(4)	0.3780(5)	0.5472(6)	1.00	0.0085(17)
O4	0.14540(32)	0.3450(4)	0.2079(8)	1.00	0.0030(19)
O5	0.3292(4)	0.31594(35)	0.2616(10)	1.00	0.0055(17)
O6	0.0450(5)	0.50	0.2691(12)	1.00	0.0055(25)
O7	0.01190(34)	0.3076(4)	0.7324(10)	1.00	0.0093(18)
Ca	0.26006(21)	0.50	0.7353(5)	1.00	0.0144(97)
W1	0.0138(18)	0.1717(7)	0.021(5)	0.428(9)	0.0244(27)
W2	0.3972(6)	0.50	0.0226(14)	1.00	0.0244(27)
W5	0.50	0.5242(19)	0.50	0.467(15)	0.0600(30)
W8	0.1414(5)	0.1194(6)	0.3574(12)	1.00	0.0600(30)

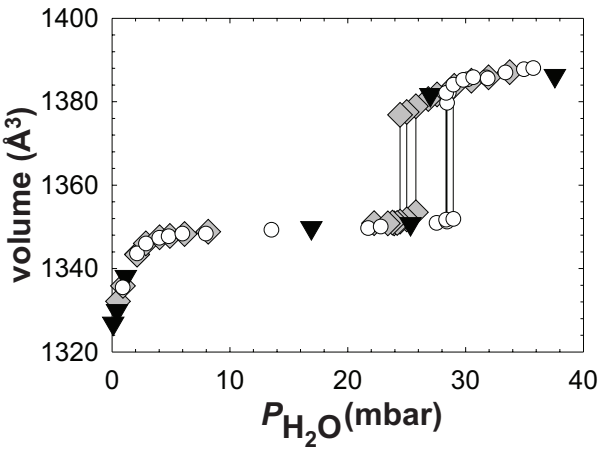

FIGURE 3. Laumontite unit-cell volume as a function of P_{H_2O} at 27.0 to 29.3 °C. Triangles represent data from detailed Rietveld refinements given in Table 1. Open circles and gray diamonds represent unit-cell volumes refined from XRD patterns collected during hydration and dehydration, respectively. Solid lines connect coexisting laumontite phases during hydration (28 to 29 mbar) and dehydration (24 to 25 mbar).

Al, which differs by ~2°.

Refined laumontite water contents (Table 1) and water site occupancies (Tables 2 to 4) as a function of water-vapor pressure demonstrate that dehydration of W1 is complete before any dehydration occurs at W5. Laumontite was nearly fully hydrated at 37.6 mbar P_{H_2O}, with 17.3 water molecules per unit cell, or slightly less than the maximum value of 18 water molecules per unit cell (Yamazaki et al. 1991; Armbruster and Kohler 1992; Artioli and Ståhl 1993). W2 and W8 were fully occupied under these conditions and W1 and W5 were 86% and 93% occupied, respectively. The W1 occupancy decreased slightly, to 80%, at 27 mbar, whereas W2 and W8 remained fully occupied and W5 nearly fully occupied. The total water content at 25.3 mbar was 13.84 molecules per unit cell. Very few changes occurred between 25.3 and 16.4 mbar; in fact, the refined total water content was slightly higher at 16.4 bar (14.09 molecules). W2, W5, and W8 were all fully occupied at 16.4 mbar but the occupancy of W1 was close to zero. We observed the first signs of dehydration at W5 at 1.2 mbar; the refined W5 occupancy was 67% of the maximum possible occupancy. The refined total water content at 0.66 and 0.11 mbar dropped to 12.7 and 12.5 water molecules per unit cell, respectively, due to further loss of water at W5. The occupancy of W5 at 0.11 mbar was 0.067, corresponding to 13% of the maximum occupancy of that site (note that the maximum occupancy of W1 and W5 is 0.5). The refined occupancy of W1 at these low water-vapor pressures was ~0.03, or 6% of the maximum occupancy. The refined total water contents of laumontite as a function of water vapor pressure are in good agreement with the gravimetric results of Yamazaki et al. (1991).

Refined unit-cell parameters as a function of P_{H_2O}

Figures 3 and 4 depict the laumontite unit-cell volume and unit-cell parameters as a function of water vapor pressure. The figures illustrate that most of the structural changes associated with the hydration/dehydration of laumontite at room temperature occurred between 0.11 and 5 mbar P_{H_2O} and above 24 mbar. These structural changes are associated with changes in the occupancy of W5 and W1, respectively. During hydration of W5 between 0.11 and 5 mbar, the volume of the unit cell expanded from 1326.9 Å^3 to 1348.8 Å^3, or by 1.7%. This volume increase was due primarily to expansion of the *c* parameter, which gradually increased from 7.452 Å to 7.555 Å over this range of water-vapor pressures. The *a* parameter expanded less, but more abruptly, from 14.705 Å at 0.11 to 14.745 Å at 2.8 mbar. Almost no change was observed in the β angle under these conditions, and the *b* parameter contracted slightly between 0.11 mbar and 2.8 mbar. Figures 3 and 4 illustrate that the structural changes associated with changes in occupancy of W5 are continuous and reversible. Unit-cell parameters refined from XRD data collected during *dehydration* of the sample are identical to those refined from data collected during *hydration*, demonstrating that the sample reached equilibrium with the controlled-*RH* atmosphere in the sample chamber within the two-hour equilibration period.

In contrast to the smooth and reversible structural changes in the low-P_{H_2O} region, structural changes associated with W1 occupancy are complex, consisting of an abrupt and hysteretic hydration/dehydration step occurring between ~24 and 29 mbar followed by continuous and gradual structural changes at higher

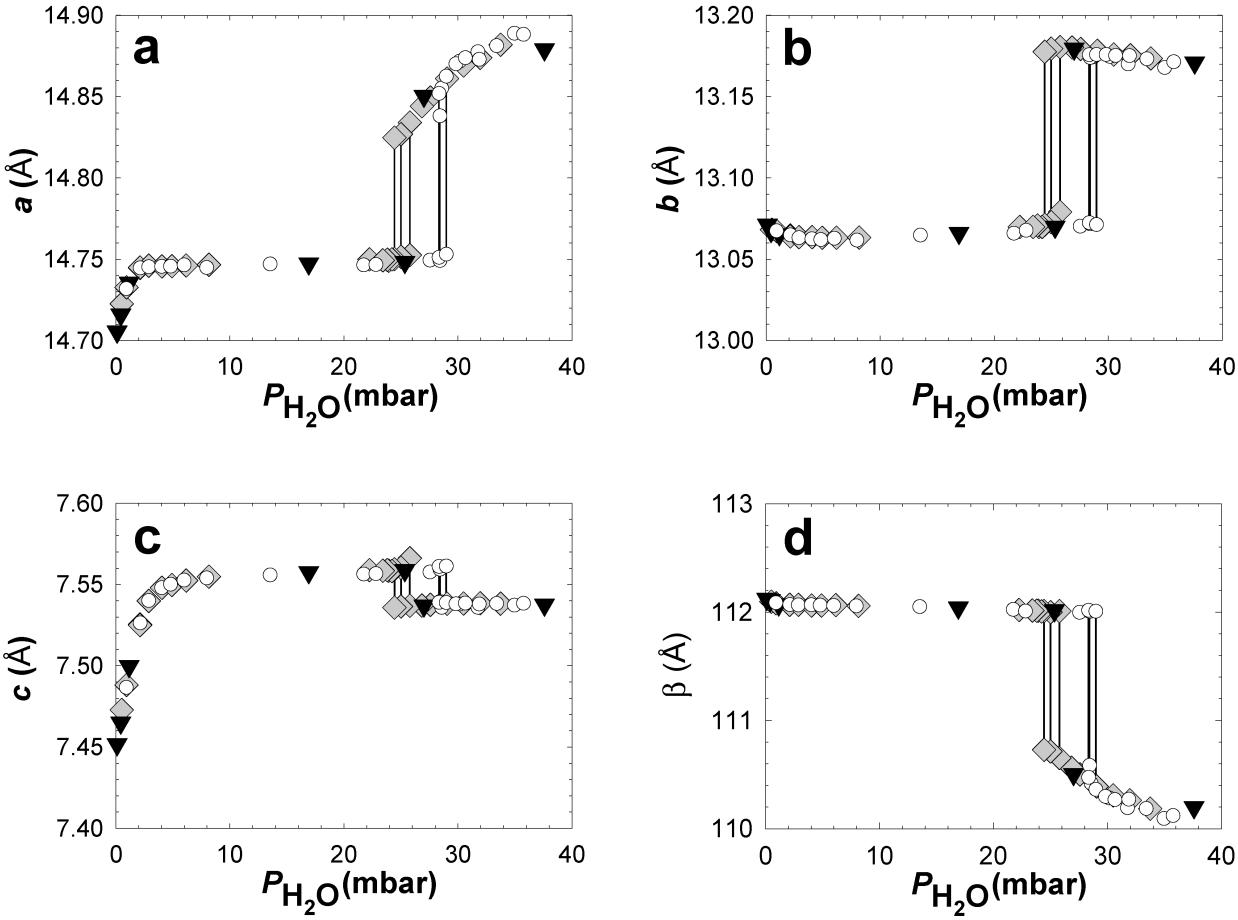

FIGURE 4. Laumontite unit-cell parameters as a function of P_{H_2O} at 27.0 to 29.3 °C. See caption to Figure 3 for explanation of symbols.

water-vapor pressures. Hysteretic behavior is obvious in this P_{H_2O} region for all unit-cell parameters as illustrated in Figures 3 and 4. During hydration of W1, the unit-cell volume increased from 1351 Å^3 to 1385 Å^3 at 28 mbar. The volume increase between 28 and 29 mbar is due to expansion of the *a* and *b* parameters by 0.12 and 0.105 Å respectively. Under these conditions, the *c* parameter contracted by 0.02 Å, in contrast to the behavior at low P_{H_2O}, and the β angle decreased from 112.0° to 110.3°. During dehydration of W1 the unit cell volume decreased from 1376 to 1350.6 Å^3 at 25 mbar, mainly due to contraction of the *a* and *b* parameters by 0.075 and 0.107 Å, respectively. At water vapor pressures above this abrupt hydration/dehydration step, the *a* parameter gradually expanded as the *b* parameter contracted and the β angle decreased in response to increased P_{H_2O}.

Figure 5, depicting a selected 2θ range (23 to 33°) of three XRD patterns measured at 27.5, 28.3, and 29.8 mbar P_{H_2O}, illustrates the discontinuous nature of the structural changes in laumontite associated with hydration/dehydration at W1. Data at 27.5 and 29.8 mbar were collected at water-vapor pressures below and above the unit-cell expansion, resulting in refined unit-cell volumes of 1350.9 Å^3 and 1385.8 Å^3, respectively. By analogy to the 25.4 mbar structure and the 27.0 mbar structure (Table 1) it can be inferred that these unit-cell volumes correspond to ~2% and ~80% occupancy of W1, respectively. These XRD patterns are shown on the bottom of the figure as a dotted curve and a black curve, respectively. The intermediate pattern, collected at 28.3 mbar, is shown above the other two patterns in the figure. Comparison of the three patterns reveals that the 28.3 mbar pattern consists of reflections from both the 27.5 mbar structure and the 29.8 mbar structure, demonstrating that the 28.3 mbar material is composed of a mixture of two laumontite phases with different unit-cell dimensions. Unit-cell parameters for the two laumontite phases were refined from the data collected at 28.3 mbar, giving unit-cell volumes of 1351.7 Å^3 and 1382.0 Å^3, respectively. Figure 5 shows that the calculated diffraction pattern for the 28.3 mbar sample based on Rietveld refinement of the two coexisting laumontite phases (shown as a solid curve) closely corresponds to the observed XRD data represented by the gray crosses. Similar "doubled" two-phase XRD patterns were also collected at 28.4 and 29.0 mbar during hydration and at 25.7, 25.0, and 24.4 mbar during dehydration. Solid lines on Figure 3 and 4 connect refined unit-cell parameters for coexisting laumontite phases. The discontinuity in unit-cell parameters between 24 and 29 mbar (Figs. 3 and 4) demonstrates that unit cells with intermediate dimensions do not exist during the transition between 24 and 29 mbar. The discontinuous nature of W1 hydration/dehydration sug-

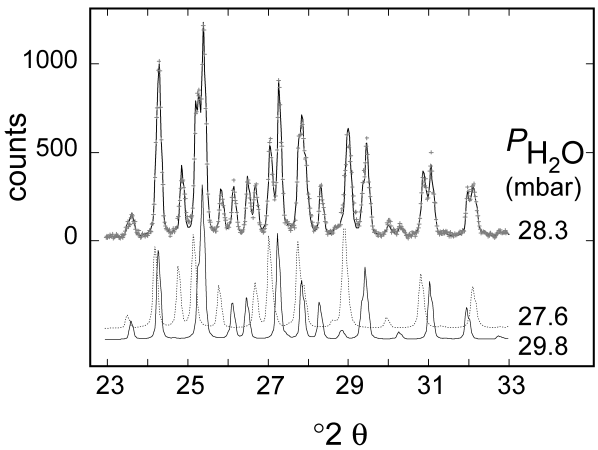

FIGURE 5. XRD patterns collected at 28.3 mbar P_{H_2O} (**top**), 27.6 mbar (**bottom**; dotted curve), and 29.8 mbar (**bottom**; solid curve). The XRD patterns at 27.6 mbar and 29.8 mbar were collected below and above the hydration of W1, respectively, whereas the 28.3 mbar pattern was collected during hydration of W1. Comparison of the 28.3 mbar pattern with the other two shows that it contains reflections from both the 27.6 mbar pattern (W1 empty) and the 29.8 mbar pattern (W1 ~80% full), thereby demonstrating the presence of two laumontite phases in the sample during hydration of W1. Individual XRD data are shown as gray crosses on the 28.3 mbar pattern, and the thick solid curve represents the theoretical XRD pattern calculated from the refined structures of two coexisting laumontite phases. Individual XRD data of the 27.6 mbar pattern and the 29.8 mbar pattern are not shown for clarity, but agreement between the data and the theoretical XRD pattern calculated for the respective refined structures was superior to that for the 28.3 mbar pattern.

gests that during hydration/dehydration of that site, W1-vacant and W1-80% occupied unit cells occur in separate domains in individual crystallites, which change their relative proportions as a function of reaction progress. Conversely, the continuous nature of hydration/dehydration at W5 indicates that vacant and occupied W5 sites are randomly distributed throughout the crystal during hydration/dehydration of that site.

Anisotropic microstrain due to changes in unit-cell parameters

Anisotropic microstrain made a considerable contribution to observed XRD peak breadths, except at intermediate vapor pressures, but peak broadening due to crystallite size was negligible. Microstrain at 27.0 and 37.6 mbar P_{H_2O} was greatest along [100], 0.45, and 0.30% respectively, and smallest parallel to [010] (~0.11%). At 0.11, 0.66, and 1.2 mbar microstrain was greatest along [001] at ~0.2%. The least microstrain was observed at 16.4 and 25.3 mbar where it was nearly isotropic at about 0.1%. That value is comparable to the minimum microstrain at both higher and lower vapor pressures and may be a result of minor chemical heterogeneity of the sample. The significant amount of microstrain along [001] at low vapor pressures correlates well with the large change in the *c* parameter as a function of vapor pressure under these conditions (Fig. 4c). Unit-cell parameters undergo little change in the 5 to 25 mbar P_{H_2O} region, accounting for the smaller and isotropic microstrain. We originally assumed that microstrain in the 25–30 mbar region would be greatest along [010] due to the large change in the *b* parameter as a function of vapor pressure in this region. The fact that microstrain was observed to be smallest along [010] and greatest parallel to [100] in this P_{H_2O} region is consistent with the *stepwise* behavior of the *b* parameter (Fig. 4b) and the vapor-pressure-dependent behavior of the *a* parameter above the hydration step (Fig. 4a).

DISCUSSION

We observed different types of behavior involving hydration/dehydration at the W1 and W5 sites in laumontite in this study. Occupancy changes at W5 as a function of vapor pressure were reversible and continuous as is typical of zeolites (Bish and Carey 2001). The reaction mechanism of W1 under our experimental conditions is a combination of both a discontinuous hydration/dehydration step between 2 and 80% occupancy and continuous hydration/dehydration above 80% occupancy, the former being typical of hydrates such as gypsum. Below we discuss a potential crystal-chemical explanation for the different hydration/dehydration reaction mechanisms involving water at these sites and consider the implications of the different types of hydration/dehydration reactions in laumontite for modeling its water content at elevated temperatures and pressures.

Effects of W1 dehydration on W2 and W8

Dehydration of W1 results in significant changes in the location of W2 and the location and shape of W8, allowing water molecules at these sites to move closer to the center of the laumontite channel. In the W1-occupied structures (i.e., the 27.0 and 37.6 mbar structures), W2 is on the [010] mirror plane, ~2.68 Å away from the W1 site (Fig. 1a). Under these conditions, the distance between the spherical W8 and W1 site is also 2.68 Å (Fig. 2b). When W1 is vacant and W5 is full (i.e., 16.4 and 27.0 mbar P_{H_2O} structures), W2 moves off the special position and splits into two 50%-occupied spherical sites (Fig. 1b) that are ~2.06 Å from the vacant W1 site. This distance between W2 and the vacant W1 site is less than the minimum distance between two occupied water sites, ~2.42 Å. Similarly, in the W1-vacant structures, the W8 site appears to become disordered or elongated with its center ~2.29 Å away from the vacant W1 site (Fig. 2c).

As noted above, the use of anisotropic displacement factors for W8, guided by Fourier difference maps (Fig. 2), substantially improved the refinement statistics for the structure models at 16.4 and 25.3 mbar. On the other hand, Fourier difference maps did not suggest significant anisotropy of the W8 site at 0.11, 0.66, 1.2, 27.0, and 37.6 mbar. The ratios of the refined anisotropic displacement factors (U_{11}, U_{22}, and U_{33}) for W8, given in Table 3 for the 16.4 mbar structure, illustrate that the site is elongated primarily along the *c* axis. The elongation of W8, which could just as well be modeled as two partially occupied, closely spaced spherical sites, is consistent with the results of both Artioli et al. (1989) and Armbruster and Kohler (1992) who observed substantial disorder of the water sites coordinating the Ca^{2+} ion in samples with ~14 H_2O per unit cell. Armbruster and Kohler (1992) refined four closely spaced, partially occupied water sites (O18, O18', O18*, and O18+) in

their *leon* sample (14.4 H_2O per unit-cell), which correspond to W8 in the present study. The locations of the four O18 sites of Armbruster and Kohler (1992) differ primarily along the *c* axis. Similarly, Artioli et al. (1989) reported several partially occupied, closely spaced sites corresponding to W8, differing in location mainly along the *c* axis in their two samples containing 13.4 and 14.2 H_2O per unit cell. Armbruster and Kohler (1992) found that the disorder of these water sites was significantly reduced at both higher (17.6 H_2O per unit cell) and lower (11.6 and 10.8 H_2O per unit cell) water contents.

Elongation or disorder of W8 along the *c* axis allows the water molecules at that site to move closer to the location of the now-vacant W1 site. This suggests a direct causal link between near complete loss of water at W1, the associated expansion of the *c* parameter (Fig. 3c), and the elongation/disorder of W8. When W1 is occupied, the water molecule of W8 is in a well-defined position, partially stabilized by hydrogen bonding to water molecules at W1. Loss of water from the W1 site leaves a vacancy in the laumontite channel that is partially compensated by elongation of W8 site toward the empty W1 site. Contraction of the unit cell along the *a* axis and particularly along the *c* axis resulting from further dehydration involving water at the W5 site restores the spherical shape of the W8 site.

Different hydration/dehydration mechanisms of W5 and W1 at room temperature

Figures 3 and 4, depicting unit-cell volume and unit-cell parameters of laumontite as a function of water-vapor pressure, illustrate the distinctly different nature of the hydration/dehydration reactions involving W1 and W5 at room temperature. During hydration/dehydration of W5 the unit-cell parameters change continuously and reversibly as a function of P_{H_2O}, indicating that the water content of W5 changes in response to infinitesimal changes in water vapor pressure at a constant temperature. This behavior is characteristic of most zeolites. The water content of zeolites is typically a continuous function of temperature or vapor pressure (Bish and Carey 2001), and consequently all intermediate compositions between the hydrated and dehydrated mineral can exist. In fact, the term "zeolitic water" is commonly used to describe molecular water in any crystallized compound that reversibly hydrates/dehydrates in response to small changes in *either* temperature *or* pressure (e.g., Boudaren et al. 2000; Jeanneau et al. 2001).

Changes in the unit-cell parameters associated with hydration/dehydration of W1 are, on the other hand, distinctly discontinuous as manifested by "doubled" or "split" XRD patterns collected during the transition (Fig. 5). The "doubled" XRD patterns demonstrate the coexistence of two laumontite phases in the sample during the hydration/dehydration of W1 and the absence of phases with intermediate unit-cell dimensions. The laumontite phase with the smaller volume had unit-cell dimensions identical to those of the 16.4 mbar structure, in which the occupancy of W1 was ~2%. The phase with the larger volume observed during hydration/dehydration of W1 had unit-cell parameters close to those of the 27.0 mbar structure, with ~80% occupancy of W1. At water-vapor pressures above the 80%-hydration level of W1 the unit-cell parameters gradually changed in response to changes in P_{H_2O}. Under these conditions, the occupancy of W1 increased from 80% at 27 mbar to 86% at 37.6 mbar. This is consistent with gravimetric observations by Yamazaki et al. (1991) showing gradual and reversible increase in water content above the abrupt hydration step at 75% *RH* at 25 °C. The absence of intermediate hydration states between 2% and 80% occupancy of W1 and discontinuous volume changes (Fig. 3) illustrate the discontinuous nature of the hydration/dehydration of W1. Above a certain minimum occupancy of W1 (~80%), hydration/dehydration of that site proceeds continuously. Comparable discontinuous hydration/dehydration reactions have not been observed in zeolites (Bish and Carey 2001) but they are characteristic of *hydrates* such as gypsum and chlorides of the alkaline earth metals, which contain water in stoichiometric quantities.

The disorder or elongation of W8 (Fig. 2b) and the relaxation of W2 toward the center of the channel due to dehydration of W1 help explain the unusual hydration/dehydration properties of W1. Because the elongation at W8 and the location of W2 in the W1-vacant structure preclude the occupancy of W1, the energetic benefit of hydration of W1 must be greater than that of W8 disorder and relocation of W2 before occupation of W1 can occur. Disordering of W8 and relaxation of W2 stabilize the W1-vacant structure to some degree, independent of P_{H_2O}, at any given temperature. The Gibbs energy of hydration of W1 is, on the other hand, a direct function of P_{H_2O}. Consequently, there is a certain P_{H_2O} at which the energetic benefits of hydration of W1 will be equal to those resulting from the disorder at W8 and relocation of W2. Under the P_{H_2O} conditions where the W1 site opens for rehydration the equilibrium occupancy of that site is ~80%. Then two laumontite phases, one with partially occupied W1, ordered W8, and W2 on a mirror plane close to the Ca^{2+} ion, and the other with vacant W1, disordered W8, and W2 on a general position relaxed toward the center of the channel, will coexist and hydration proceeds as a discontinuous, univariant reaction. Once partial occupancy of the W1 site has been established, the locations of W8 and W2 no longer prevent water molecules from entering W1 so the remaining hydration of W1 will proceed in a continuous fashion. However, it remains unclear why W1-occupied and W1-vacant unit cells are incompatible with each other, i.e., that they occur in separate domains and not randomly distributed throughout the crystal.

Loss of water from the W5 site (0.11 and 0.66 mbar structures) does not significantly affect the positions of the W2 and W8 sites. Consequently, water molecules can move unobstructed into the vacant W5. This explains how the occupancy of W5 can change continuously and reversibly in response to minor changes in vapor pressure, in contrast to the discontinuous occupancy changes of W1 as a function of vapor pressure.

Mechanisms of W1 hydration/dehydration at elevated temperatures

Accurate predictions of laumontite phase relations at elevated temperatures and pressures rely on precise knowledge of its water content as a function of temperature and pressure. As a result of the small entropies and volumes of univariant reactions defining laumontite stability in geologic systems, erroneous water stoichiometry can greatly affect predicted

Clapeyron slopes of these reactions (Neuhoff et al. 2000). Consequently, the nature of the hydration/dehydration reactions at W1 and W5 will have important implications for thermodynamic modeling of laumontite parageneses under petrogenetic conditions.

Neuhoff and Bird (2001) modeled W1 hydration/dehydration as a univariant reaction, with W1 completely occupied at the low-temperature side of the reaction and W1 vacant on the high-temperature side, i.e., a discontinuous reaction. Their choice of reaction mechanism for W1 hydration/dehydration was based on the shape of the gravimetric water-adsorption isotherm reported by Yamazaki et al. (1991) who conducted their experiments under conditions similar to those of the present study. Thermodynamic calculations by Neuhoff and Bird (2001) demonstrated that experimental and geologic phase relations between stilbite, heulandite, and laumontite were incompatible with the water stoichiometry of fully hydrated laumontite but were consistent with partially dehydrated laumontite containing ~14 H_2O per unit cell, i.e., laumontite with a completely vacant W1 site at temperatures as low as ~80 °C. Complete dehydration of W1 at such low temperatures is difficult to explain if W1 dehydration proceeds as a continuous reaction, but it is consistent with the discontinuous nature of W1 hydration/dehydration observed in this study. Further support for a discontinuous W1 hydration/dehydration reaction under water-saturated conditions is provided by van Reeuwijk (1974) who observed that heating a wetted laumontite sample resulted in abrupt evolution of liquid water at 57 °C when "leonhardite" was formed. He did not use the term "discontinuous reaction" to describe the laumontite-to-"leonhardite" dehydration reaction but he did point out the analogy to salt hydrates where this behavior has been described. He also suggested the presence of a "quadruple point in the laumontite system" where "four phases may co-exist viz., laumontite, leonhardite, H_2O (l) and H_2O (g)" (van Reeuwijk 1974).

Ståhl et al. (1996) showed that the site occupancy of W1 decreased *continuously* from 3.44 H_2O per unit cell at 37 °C to 0.36 H_2O per unit cell at 76 °C while the sample was submerged in water, in contrast to the results of this study, experimental observations reported by van Reeuwijk (1974), and thermodynamic calculations by Neuhoff and Bird (2001). Furthermore, their refined unit-cell parameters changed *continuously* during dehydration of W1 (Ståhl et al. 1996), indicating that dehydration of W1 proceeds continuously as a function of temperature in the presence of liquid water. To investigate whether this discrepancy between the results of Ståhl et al. (1996) and our results were due to different properties of the natural laumontite samples used in the two studies, we conducted complementary experiments with the laumontite sample used by Ståhl et al. (1996), which was graciously provided by G. Artioli. We found that their laumontite sample behaved very much as the Drain County, Oregon, sample, i.e., we observed "doubled" XRD patterns during dehydration of W1, confirming that the different dehydration mechanisms are due to the different experimental conditions (P_{H_2O} and temperature) and not to inherent differences in the samples used in the two studies. This may suggest a possible solvus in the solid solution between laumontite with vacant W1 and laumontite with ~80% occupied W1 at ~28 °C and 0 to 37 mbar P_{H_2O} (this study) that was not encountered under the experimental conditions of Ståhl et al. (1996). However, van Reeuwijk's (1974) observation of discontinuous dehydration of laumontite was made under water-saturated conditions, similar to those of Ståhl et al. (1996), leaving the contrasting observations of these two studies unexplained.

Hydration/dehydration of W5 is a continuous reaction and the water occupancy of this site is thus appropriately modeled with a Langmuir adsorption model (c.f. Carey and Bish 1996; Bish and Carey 2001). The results of this study, calculations by Neuhoff and Bird (2001), and experimental observations by van Reeuwijk (1974) suggest that W1 hydration/dehydration should be modeled as a discontinuous, univariant reaction under geologic conditions. However, if W1 hydration/dehydration is a discontinuous reaction, as suggested by the data of Ståhl et al. (1996), the occupancy of W1 would be more appropriately modeled with a Langmuir adsorption model resulting in a series of isopleths of constant occupancy of W1 over the *P-T* conditions where laumontite occurs. Experimentally determined thermodynamic properties of hydration of W1 will be reported in the second part of this study and there we discuss the petrogenetic implications of different approaches to modeling the occupancy of W1.

ACKNOWLEDGMENTS

We thank C. Jove for donating the experimental material via P. Neuhoff, G. Artioli for providing a portion of the laumontite sample used in several XRD studies by him and his coworkers, S. Chipera for logistical help with the XRD experiments, and P. Snow for assistance with the electron microprobe analyses. Sample preparation was conducted in part at Lawrence Livermore National Laboratory, with the assistance of R. Pletcher and B. Viani. Conversations with W. Carey and P. Neuhoff contributed significantly to the development of this work. A review of an early version of the manuscript by A. Spieler was helpful, and reviews by P. Neuhoff, G. Artioli, and an anonymous reviewer significantly improved the manuscript. Funding for this project was provided by a Los Alamos National Laboratory Institute of Geophysics and Planetary Physics grant, number 1108, to D. L. Bish and D. K. Bird, and a grant from the National Science Foundation (NSF EAR 0001113) to D. K. Bird.

REFERENCES CITED

Alberti, A. and Gottardi, G. (1988) The determination of the Al-content in the tetrahedra of framework silicates. Zeitschrift für Kristallographie, 184, 49–61.

Armbruster, T. and Kohler, T. (1992) Rehydration and dehydration of laumontite: a single-crystal X-ray study at 100-K. Neues Jahrbuch für Mineralogie Monatshefte, 9, 385–397.

Artioli, G. and Ståhl, K. (1993) Fully hydrated laumontite: a structure study by flat-plate and capillary powder diffraction techniques. Zeolites, 13, 249–255.

Artioli, G., Smith, J.V., and Kvick, A. (1989) Single-crystal neutron-diffraction study of partially dehydrated laumontite at 15K. Zeolites, 9, 377–391.

Bish, D.L. and Carey, J.W. (2001) Thermal behavior of natural zeolites. In D.L. Bish, and D.W. Ming, Eds., Natural Zeolites: Occurrence, Properties, Applications, 45. Mineralogical Society of America.

Boudaren, C., Auffredic, J.P., Louer, M., and Louer, D. (2000) Synthesis, structure determination from powder diffraction data, and thermal behavior of lead zirconium oaxalate hydrate $Pb_2Zr(C_2O_4)_4{\cdot}nH_2O$ ($3 < n < 9$). Chemistry of Materials, 12, 2324–2333.

Carey, J.W. and Bish, D.L. (1996) Equilibrium in the clinoptilolite-H_2O system. American Mineralogist, 81, 952–962.

Chipera, S.J., Carey, J.W., and Bish, D.L. (1997) Controlled-humidity XRD analyses: Application to the study of smectite clay expansion/contraction. In J.V. Gilfrich, Ed., Advances in X-ray Analysis, 39. Plenum Press, New York.

Coombs, D.S. (1952) Cell size, optical properties, and chemical composition of laumontite and leonhardite. American Mineralogist, 37, 812–830.

Coombs, D.S., Ellis, A.J., Fyfe, W.S., and Taylor, A.M. (1959) The zeolite facies, with comments on the interpretation of hydrothermal syntheses. Geochimica et Cosmochimica Acta, 17, 53–107.

Coombs, D.S., Alberti, A., Armbruster, T., Artioli, G., Colella, C., Galli, E., Grice, J.D., Liebau, F., Mandarino, J.A., Minato, H., Nickel, E.H., Passaglia, E., Peacor,

D.R., Quartieri, S., Rinaldi, R., Ross, M., Sheppard, R.A., Tillmanns, E., and Vezzalini, G. (1997) Recommended nomenclature for zeolite minerals: Report of the subcommittee on zeolites of the International Mineralogical Association, Commission on New Minerals and Mineral Names. Canadian Mineralogist, 35, 1571–1606.

Fridriksson, Th., Neuhoff, P.S., Arnórsson, S., and Bird, D.K. (2001) Geological constraints on the thermodynamic properties of the stilbite-stellerite solid solution in low-grade metabasalts. Geochimica et Cosmochimica Acta, 65, 3993–4008.

Iijima, A. (1978) Geological occurrences of zeolite in marine environments. In L.B. Sand, and F.A. Mumpton, Eds., Natural Zeolites, p. 175–198. Pergamon Press Ltd., Oxford.

———(1988) Diagenetic transformations of minerals as exemplified by zeolites and silica minerals; a Japanese view. In G.V. Chilingarian, Ed., Diagenesis II: Developments in Sedimentology, 43, p. 147–209. Elsevier, Amsterdam-Oxford-New York.

Jeanneau, E., Audebrand, N., Auffredic, J.P., and Louer, D. (2001) Crystal structure, thermal behaviour and zeolitic properties of $Cd_2Zr(C_2O_4)_4{\cdot}(4+n)H_2O$. Journal of Materials Chemistry, 11, 2545–2552.

Kiseleva, I., Navrotsky, A., Belitsky, I.A., and Fursenko, B.A. (1996) Thermochemistry and phase equilibria in calcium zeolites. American Mineralogist, 81, 658–667.

Larson, A.C. and Von Dreele, R.B. (2000) General Structure Analyses System (GSAS). Los Alamos National Laboratory Report LAUR, 86–748.

Murata, K.J., Formoso, M.L.L., and Roisenberg, A. (1987) Distribution of zeolites in lavas of southeastern Parana Basin, State of Rio-Grande-Do-Sul, Brazil. Journal of Geology, 95, 455–467.

Neuhoff, P.S. and Bird, D.K. (2001) Partial dehydration of laumontite: thermodynamic constraints and petrogenetic implications. Mineralogical Magazine, 65, 59–70.

Neuhoff, P.S., Watt, W.S., Bird, D.K., and Pedersen, A.K. (1997) Timing and structural relations of regional zeolite zones in basalts of the East Greenland continental margin. Geology, 25, 803–806.

Neuhoff, P.S., Fridriksson, Th., Arnórsson, S., and Bird, D.K. (1999) Porosity evolution and mineral paragenesis during low-grade metamorphism of basaltic lavas at Teigarhorn, eastern Iceland. American Journal of Science, 299, 467–501.

Neuhoff, P.S., Fridriksson, Th., and Bird, D.K. (2000) Zeolite parageneses in the North Atlantic igneous province: Implications for geotectonics and groundwater quality of basaltic crust. International Geology Review, 42, 15–44.

Paukov, I.E. and Fursenko, B.A. (1998a) Low-temperature heat capacity and thermodynamic functions of leonhardite. Geochemistry International, 36, 471–473.

——— (1998b) Low-temperature heat capacity and thermodynamic properties of laumontite. Geochemistry International, 36, 1177–1179.

Pouchou, J.L. and Pichoir, F. (1984) A new model for quantitative analysis: Part I. Application to the analysis of homogenous samples, La Recherche Aerospatiale, 3, 13–38.

Schmidt, S.Th. (1990) Alteration under conditions of burial metamorphism in the North Shore Volcanic Group, Minnesota—Mineralogical and geochemical zonation. 309 p. Heidelberger Geowissenschaftliche Abhandlungen, Heidelberg.

Ståhl, K. and Artioli, G. (1993) A neutron powder diffraction study of fully deuterated laumontite. European Journal of Mineralogy, 5, 851–856.

Ståhl, K., Artioli, G., and Hanson, J.C. (1996) The dehydration process in the zeolite laumontite: A real-time synchrotron X-ray powder diffraction study. Physics and Chemistry of Minerals, 23, 328–336.

Sukheswala, R.N., Avasia, R.K., and Gangopadhyay, M. (1974) Zeolites and associated secondary minerals in the Deccan Traps of West India. Mineralogical Magazine and Journal of the Mineralogical Society, 39, 658–671.

van Reeuwijk, L.P. (1974) The thermal dehydration of natural zeolites. H. Veenman and Zonen B.V. Wageningen, The Netherlands.

Yamazaki, A., Shiraki, T., Nishido, H., and Otsuka, R. (1991) Phase change of laumontite under relative humidity-controlled conditions. Clay Science, 8, 79–86.

MANUSCRIPT RECEIVED MAY 20, 2002
MANUSCRIPT ACCEPTED OCTOBER 4, 2002
MANUSCRIPT HANDLED BY DAVID COLE